Exponential Distance Dependence of Photoinitiated Stepwise Electron Transfer in Donor–Bridge–Acceptor Molecules: Implications for Wirelike Behavior

ARTICLE *in* JOURNAL OF THE AMERICAN CHEMICAL SOCIETY · MARCH 2012

Impact Factor: 12.11 · DOI: 10.1021/ja205913q · Source: PubMed

7 AUTHORS, INCLUDING:

Matthias Wenninger
Ludwig-Maximilians-University of Munich
6 PUBLICATIONS **87** CITATIONS
SEE PROFILE

Yuri Berlin
Northwestern University
121 PUBLICATIONS **2,719** CITATIONS
SEE PROFILE

Dick Co
Northwestern University
20 PUBLICATIONS **593** CITATIONS
SEE PROFILE

JACS
JOURNAL OF THE AMERICAN CHEMICAL SOCIETY
Article
pubs.acs.org/JACS

Exponential Distance Dependence of Photoinitiated Stepwise Electron Transfer in Donor–Bridge–Acceptor Molecules: Implications for Wirelike Behavior

Annie Butler Ricks, Kristen E. Brown, Matthias Wenninger, Steven D. Karlen, Yuri A. Berlin, Dick T. Co,* and Michael R. Wasielewski*

Department of Chemistry and Argonne–Northwestern Solar Energy Research (ANSER) Center, Northwestern University, Evanston, Illinois 60208-3113, United States

Supporting Information

ABSTRACT: Donor–bridge–acceptor (D–B–A) systems in which a 3,5-dimethyl-4-(9-anthracenyl)julolidine (DMJ-An) chromophore and a naphthalene-1,8:4,5-bis(dicarboximide) (NI) acceptor are linked by oligomeric 2,7-fluorenone (FN_n) bridges (n = 1–3) have been synthesized. Selective photoexcitation of DMJ-An quantitatively produces $DMJ^{+\bullet}$-$An^{-\bullet}$, and $An^{-\bullet}$ acts as a high-potential electron donor. Femtosecond transient absorption spectroscopy in the visible and mid-IR regions showed that electron transfer occurs quantitatively in the sequence: $DMJ^{+\bullet}$-$An^{-\bullet}$–FN_n–NI → $DMJ^{+\bullet}$-An–$FN_n^{-\bullet}$–NI → $DMJ^{+\bullet}$-An–FN_n–$NI^{-\bullet}$. The charge-shift reaction from $An^{-\bullet}$ to $NI^{-\bullet}$ exhibits an exponential distance dependence in the nonpolar solvent toluene with an attenuation factor (β) of 0.34 $Å^{-1}$, which would normally be attributed to electron tunneling by the superexchange mechanism. However, the $FN_n^{-\bullet}$ radical anion was directly observed spectroscopically as an intermediate in the charge-separation mechanism, thereby demonstrating conclusively that the overall charge separation involves the incoherent hopping (stepwise) mechanism. Kinetic modeling of the data showed that the observed exponential distance dependence is largely due to electron injection onto the first FN unit followed by charge hopping between the FN units of the bridge biased by the distance-dependent electrostatic attraction of the two charges in $D^{+\bullet}$–$B^{-\bullet}$–A. This work shows that wirelike behavior does not necessarily result from building a stepwise, energetically downhill redox gradient into a D–B–A molecule.

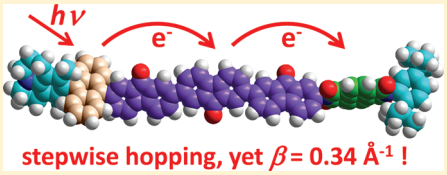

INTRODUCTION

Achieving distance-independent "wirelike" electron transfer in molecular donor–bridge–acceptor (D–B–A) systems requires a detailed understanding of how electron transfer depends on molecular structure.[1] Systematic studies of electron transfer involving covalently linked D–B–A systems have examined a variety of bridge molecules, including DNA base pairs;[2] peptides in proteins;[3] porphyrins;[4] saturated alkane σ systems;[5] and unsaturated alkene, alkyne, and aromatic π-conjugated spacers.[6] In most of these D–B–A systems, electron transfer from D to A occurs by the coherent superexchange mechanism, which involves mixing of virtual states having charge formally on the bridge with the initial donor state and requires the virtual bridge states to be energetically much higher in energy than the donor state. McConnell used second-order perturbation theory to derive an expression for the bridge-mediated electronic coupling V_{DA} between D and A with identical B units that mediate the electronic coupling:[7]

$$V_{DA} = \frac{V_{DB}V_{BA}}{\Delta E_{DB}}\left(\frac{V_{BB}}{\Delta E_{DB}}\right)^{n-1} \quad (1)$$

where V_{DB} and V_{BA} are the matrix elements that couple D to B and B to A, respectively, n is the number of identical B units, V_{BB} is the electronic coupling between B units, and ΔE_{DB} is the energy gap between the donor and bridge states. When $V_{BB} \ll \Delta E_{DB}$, the distance dependence of the electronic coupling is described by

$$V_{DA} = V_0 e^{-\beta(R-R_0)/2} \quad (2)$$

where V_0 is the coupling at the van der Waals contact distance R_0, R is the D–A distance, and β is the attenuation factor, given by eq 3:

$$\beta = \frac{2}{r}\ln\left|\frac{\Delta E_{DB}}{V_{BB}}\right| \quad (3)$$

in which r is the length of one bridge segment. Since theory shows that the electron-transfer rate constant k_{DA} is proportional to V_{DA}^2,[8] the distance dependence of k_{DA} via the coherent superexchange mechanism is exponential and is given by[2a,9]

$$k_{DA} = k_0 e^{-\beta(R-R_0)} \quad (4)$$

When the energies of the virtual states having charge on the bridge become resonant with that of the initial state or drop below it, the bridge states become real, and incoherent charge hopping from one distinct redox site to the next can occur.[10]

Received: June 24, 2011
Published: February 15, 2012

   dx.doi.org/10.1021/ja205913q | J. Am. Chem. Soc. 2012, 134, 4581–4588

Under these conditions, the perturbation theory assumptions inherent in the superexchange mechanism break down, and the observed small β values are strictly phenomenological. Thus, depending on the energies of the charge-separated states involving the bridge molecules, the incoherent hopping mechanism should become more efficient than the coherent superexchange process at long distances, so measurements of the distance dependence of the electron-transfer rate are often employed to differentiate between these mechanisms. Charge transport within π-linked D−B−A molecules has been studied under a variety of conditions[2−4,5b,6d,11] to identify the molecular properties that determine the crossover from superexchange to hopping when molecular systems exhibit a combination of these mechanisms.[7,12] However, lengthening the bridge often changes other system parameters, such as bridge redox potentials and molecular conformations.[6c] Nevertheless, the shallow distance dependence of the charge-hopping mechanism should be favorable for constructing a molecular wire that allows efficient electron transfer over long distances.

While determining β has been the object of many experimental[6d,11b,13] and theoretical[14] studies, concerns have been raised as to the reliability of β in assessing the role of superexchange in a given electron-transfer reaction.[15] The observed β values for π-conjugated bridges range from those characteristic of fully conducting bridges (β close to zero) to those of nearly insulating ones ($\beta > 0.5$ Å^{-1}), while σ bridges have very high β values near unity.[15b] By convention, $\beta = 0.2-0.3$ Å^{-1} is considered to be the lower limit of the superexchange regime, with lower values attributed to a significant contribution from the incoherent hopping mechanism.[14a,b] For D−B−A systems in which the charge-hopping mechanism is operative, it is difficult to assign an upper limit to the observed phenomenological β value because several potential mechanisms can result in such behavior, which is the principal focus of this paper.

For sufficiently long bridges, theory has identified three conditions under which the incoherent hopping mechanism can exhibit an exponential distance dependence with a β value similar to that for the single-step coherent superexchange mechanism.[14] In general, these conditions all reflect an asymmetry in the hopping rates between bridge sites in the forward (toward A) and backward (toward D) directions and/or the competition of hopping with different channels for charge depopulation of the bridge.[14] First, if the charge-hopping rates between independent bridge sites are the same, a significant difference in the rates of charge recombination from the bridge to the donor and charge trapping by the terminal acceptor can lead to a large β value. Second, the distance-dependent electrostatic attraction of the two charges in $D^{+\bullet}-B^{-\bullet}-A$ can provide asymmetries in the rate constants that lead to significant β values.[14a] Third, injection of the electron onto the bridge may result in polaron formation resulting from significant charge delocalization over multiple bridge sites along with the structural and solvent distortions that accompany it, which may result in significant β values.[16]

We now report on a series of D−B−A molecules for which we have experimentally shown the electron transfer to proceed solely by stepwise, incoherent hopping yet exhibit a significant β value in a nonpolar solvent. Previous studies of D−B−A systems with reported β values as high as 1.47 Å^{-1}, which were attributed to the hopping mechanism, mostly involved charge transport in DNA, where the polar solvent (water) and counterions provided a means for polaron-like hopping.[17] Utilizing femtosecond visible pump/visible probe and visible pump/mid-IR probe transient absorption spectroscopies, we have unequivocally identified the reduced bridge as an intermediate in the charge-transfer process and determined the charge separation time as a function of the D−A distance using distinctive spectroscopic tags for the electron arrival at the acceptor. The D−B−A system that we employed consists of an anthracene radical anion electron donor produced by photoexcitation of 3,5-dimethyl-4-(9-anthracenyl)julolidine (DMJ-An) to its charge-transfer state, $DMJ^{+\bullet}$-$An^{-\bullet}$; a series of fluorenone oligomers FN_n (n = 1−3) as the bridges; and naphthalene-1,8:4,5-bis(dicarboximide) (NI) as the electron acceptor (Figure 1). Photoexcitation of DMJ-An produces

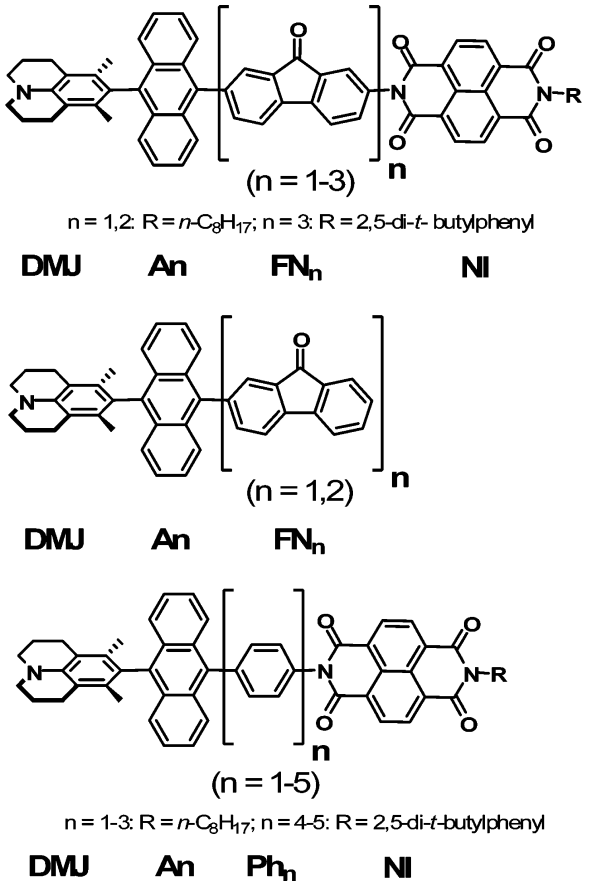

Figure 1. (top) D−B−A molecules and (center) model compounds used in this study. Results were compared to the (bottom) analogous molecules studied previously.[25]

$DMJ^{+\bullet}$-$An^{-\bullet}$ quantitatively,[17] and $An^{-\bullet}$ acts as a high-potential electron donor. The FN_n bridges are advantageous because their reduction potentials change only modestly as n increases (−1.27, −1.14, and −1.08 V vs SCE for n = 1−3, respectively; see the Supporting Information). The aforementioned hopping mechanisms are discussed below along with comparisons with the coherent superexchange mechanism.

EXPERIMENTAL SECTION

Synthesis. The synthesis and characterization of DMJ-An−FN_n−NI (n = 1−3) were reported earlier,[18] while those of DMJ-An−FN_n (n = 1, 2) are described in the Supporting Information. All reagents were purchased from Sigma-Aldrich and used as received. All final products were purified by normal-phase preparative thin-layer chromatography prior to characterization. All solvents were spectrophotometric grade

or distilled prior to use. Intermediates and the resulting products were characterized by ^{1}H NMR and UV−vis spectroscopy and high-resolution mass spectrometry.

Optical Spectroscopy. Steady-state absorption spectroscopy was performed using a Shimadzu UV-1800 spectrophotometer. All solvents were spectroscopic grade and used as received, except for tetrahydrofuran (THF) and toluene, which were further purified through a GlassContour solvent system immediately prior to use. Spectroelectrochemistry was carried out in argon-purged *N*,*N*-dimethylformamide (DMF) with 0.1 M Bu_4NPF_6 as the supporting electrolyte. Bulk electrolysis was performed using a computer-controlled potentiostat (CH Instruments) and a three-electrode arrangement in a 2 mm glass cuvette utilizing a platinum wire mesh working electrode, a platinum wire auxiliary electrode, and a silver wire pseudoreference electrode. The cuvette was placed in a computer-controlled spectrophotometer (Shimadzu UV-1800). Spectra of the electrochemically generated anions were recorded by passing the light from the spectrophotometer through the platinum mesh and sweeping from 800 to 350 nm every 2 min. A blank spectrum consisting of the cuvette filled with solvent and supporting electrolyte was subtracted from each data set.

Femtosecond visible pump/visible probe transient absorption measurements were made using the 416 nm frequency-doubled output from a 2 kHz regeneratively amplified Ti:sapphire laser system as the pump.[6a] A white-light-continuum probe pulse was generated by focusing the IR fundamental into a 1 mm sapphire disk.[19] Detection with a charge-coupled device (CCD) spectrograph has been described previously.[19] The optical density of all samples was maintained between 0.3 and 0.5 at 416 nm. The samples were placed in a 2 mm path length quartz cuvette equipped with a vacuum adapter and subjected to five freeze−pump−thaw degassing cycles prior to transient absorption measurements. The samples were irradiated with 1.0 μJ, 416 nm laser pulses focused to a 200 μm spot. Typically, 5−7 s of averaging was used to obtain the transient spectrum at a given delay time. The total instrument response function (IRF) for the pump−probe experiments was 150 fs. The transient absorption kinetics at a given wavelength was determined by using a nonlinear least-squares fit to a general sum of exponentials (Levenberg−Marquardt algorithm) convolved with a Gaussian function to account for the finite instrument response. The three-dimensional (3D) data set (ΔA vs time and wavelength) was analyzed using global fitting to obtain decay-associated difference spectra (DADS) (see the Supporting Information).

Femtosecond visible pump/mid-IR probe transient absorption spectroscopy was performed on DMJ-An−FN_n (n = 1, 2) and DMJ-An−FN_2−NI. The data were obtained in THF because toluene is too absorptive in the 1500−1800 cm^{-1} spectral region. Complementary femtosecond visible transient absorption data in THF were also obtained for direct comparison with the transient IR results. The femtosecond IR transient absorption setup was based on a 1 kHz Ti:sapphire regenerative amplifier (Spitfire Pro, Spectra-Physics) seeded by a Ti:sapphire oscillator (Tsunami, Spectra-Physics). The 1 mJ, 45 fs output of the amplifier was split into two beams of equal energy that were used to pump two separate optical parametric amplifiers (TOPAS-C, Light Conversion) to generate the tunable visible pump (290−2600 nm) and mid-IR probe (1000−4000 cm^{-1}) pulses. A gradient neutral-density filter wheel was used as the first turning mirror in the mid-IR beam path. By adjustment of the amount of reflectance, the intensity of the mid-IR probe pulse could be attenuated to a level below the detector saturation limit. The mid-IR beam was then split into vertically displaced probe and reference beams before the sample with a wedged ZnSe window, and multichannel detection of the ∼400 cm^{-1} bandwidth IR probe light was achieved using a dual-array, 2 × 64-element mercury cadmium telluride (MCT) detector (InfraRed Associates, Inc.). The 400 nm pump pulse was produced from the 800 nm fundamental by second-harmonic generation, chopped at 500 Hz, and sent down an optical delay line before being focused at the sample with a 10 cm off-axis silver parabolic mirror along with the probe and reference beams. The probe beam was horizontally polarized, and the pump beam polarization was set to the magic angle (54.7°) to eliminate contributions from rotational motion of the molecule in solution. The IRF was ∼300 fs. The sample cell consisted of a 2 mm Teflon spacer between two 2 mm thick CaF_2 windows (Harrick Scientific Products, Inc.). The pump beam was rejected with an iris after passing through the sample, and the probe and reference beams were dispersed by an imaging spectrometer (Triax 190, HORIBA Jobin Yvon) equipped with a 75 groove/mm grating. Typically ∼250 cm^{-1} of mid-IR light was imaged onto the 64 pixels of the MCT detector. However, our data in the same spectral window had three times the density of pixels as a result of interleaving of the spectra obtained at three grating positions and reconstitution of the recorded spectrum. Each time point was the sum of three spectra, each of which was obtained after 4 s of averaging.

RESULTS

Steady-State Spectroscopy. The ground-state absorption spectrum of DMJ-An in toluene exhibits a broad charge-transfer absorption maximum at 367 nm with a broad emission maximum at 519 nm, resulting in an excited singlet charge-transfer state with an energy of 2.89 eV.[17,20] The ground-state absorption spectra of DMJ-An−FN_n−NI and DMJ-An−FN_n have absorption maxima at 360 and 380 nm and a shoulder at 398 nm, with the prominent vibronic structure coming from overlapping contributions of the DMJ-An charge-transfer absorption and the NI acceptor Franck−Condon progression (Figure 2). As the bridge length increases, additional broad

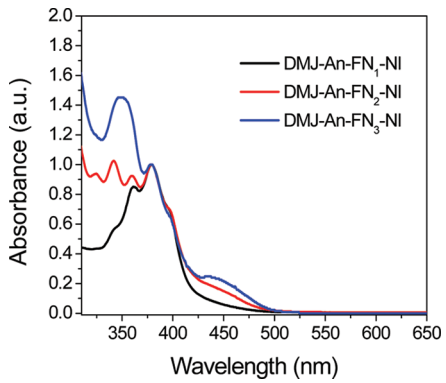

Figure 2. Ground-state absorption spectra of DMJ-An−FN_n−NI (n = 1−3) normalized at 380 nm.

features resulting from the increased conjugation of the FN bridging units appear between 300 and 360 nm, along with a weak band at 450 nm whose intensity grows in proportion to the length of the bridge, which is assigned to FN_n.[21]

Ion-Pair Distances and Energies. Given that photoexcitation of DMJ-An results in quantitative subpicosecond charge separation to produce DMJ$^{+\bullet}$-An$^{-\bullet}$ with a spectroscopically determined energy of 2.89 eV in toluene,[17,20] the energy levels for the charge-separated states DMJ$^{+\bullet}$-An−$FN_n^{-\bullet}$−NI and DMJ$^{+\bullet}$-An−FN_n−NI$^{-\bullet}$ were determined in toluene using eq 5:

$$\Delta G_F = \Delta G_I + \mathrm{sign}(E_I - E_F) + \frac{e^2}{\varepsilon_S}\left(\frac{1}{r_I} - \frac{1}{r_F}\right) \quad (5)$$

where ΔG_I and ΔG_F are the energies above ground state for the initial and final ion pairs, respectively, E_I and E_F are the redox potentials for the initial and final ions between which the electron is transferred, respectively, r_I and r_F are the initial and final ion-pair distances, respectively, e is the electron charge, ε_S

dx.doi.org/10.1021/ja205913q | J. Am. Chem. Soc. 2012, 134, 4581−4588

is the static dielectric constant of the solvent (2.38 for toluene), and sign($E_I - E_F$) is negative when $E_F > E_I$ and positive when $E_I > E_F$. The parameters used in eq 5 are listed in Table S1 in the Supporting Information, and the energy levels of the relevant states are illustrated in Figure 3 and listed in Table S2.

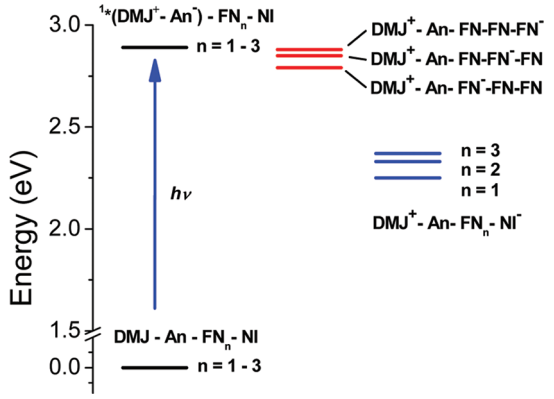

Figure 3. Energy levels for the electronic states relevant to the electron-transfer pathways for DMJ-An−FN$_n$−NI (n = 1−3), as determined by eq 5.

Visible Transient Absorption Spectroscopy. The data in Figure 3 show that the reaction DMJ$^{+\bullet}$-An$^{-\bullet}$−FN$_n$−NI → DMJ$^{+\bullet}$-An−FN$_n^{-\bullet}$−NI leading to the reduction of the FN$_n$ bridge is exergonic for n = 1−3. To test this result, model compounds DMJ-An−FN$_n$ (n = 1, 2) consisting of only the donor and bridge were studied. Their ground-state absorption spectra are shown in Figure S1 in the Supporting Information. DMJ-An−FN$_3$ proved to be very insoluble and was not examined. Femtosecond transient absorption spectra in toluene were recorded using 416 nm pulses to excite the charge-transfer band of DMJ-An.[18] The relative extinction coefficients of FN$_n$ (n = 1−3) versus DMJ-An at 416 nm result in ∼70% selective excitation of DMJ-An. Since the energy of the lowest excited singlet state of DMJ-An is lower than those of FN$_n$ (n = 1−3), energy transfer from FN$_n$ to DMJ-An likely occurred within the 150 fs IRF, as the transient spectra at the earliest time points strongly resemble that of DMJ$^{+\bullet}$-An$^{-\bullet}$, with a more intense band in the red (λ > 600 nm) than in the blue (λ < 500 nm).[22] The 3D data sets (ΔA vs time and wavelength) were analyzed using global fitting to obtain the DADS that are shown in Figure 4 along with the spectroelectrochemical spectra for FN$_1^{-\bullet}$ and FN$_2^{-\bullet}$. The DADS for DMJ-An−FN$_1$ shows two bands at ∼485 and 572 nm, while that for DMJ-An−FN$_2$ shows two bands at ∼485 and 606 nm. The band near 485 nm is assigned to DMJ$^{+\bullet}$,[22] while the 572 and 606 nm bands are assigned to FN$_1^{-\bullet}$ and FN$_2^{-\bullet}$, respectively, on the basis of the spectra of FN$_1^{-\bullet}$ (560 nm) and FN$_2^{-\bullet}$ (579 nm) determined by spectroelectrochemistry in DMF (Figure 4). The modest red shift of the transient absorption maximum of FN$_2^{-\bullet}$ relative to that of FN$_1^{-\bullet}$ (34 nm for the transient spectra in toluene and 19 nm for the spectroelectrochemical data in DMF) is consistent with the presence of an electronic interaction between the two FN bridge units within FN$_2^{-\bullet}$. The global fits yielded a charge-separation time constant (τ_{CS}) of 21 ps and a charge-recombination lifetime (τ_{CR}) of 6.0 ns for DMJ-An−FN$_1$ and gave τ_{CS} = 30 ps and τ_{CR} = 3.9 ns for DMJ-An−FN$_2$.

Transient absorption measurements on DMJ-An−FN$_n$−NI (n = 1−3) were performed under the same conditions (Figure 5). The transient spectra show the formation of 480 nm (ε = 26 000 M^{-1} cm^{-1}) and 610 nm (ε = 7200 M^{-1} cm^{-1}) absorption bands characteristic of NI$^{-\bullet}$.[23] In comparison, the DMJ$^{+\bullet}$ absorption at 485 nm is weak (ε_{max} = 4500 M^{-1} cm^{-1})[22] and overlaps with that of NI$^{-\bullet}$, and therefore, it could not be observed distinctly. Additional broad features were observed at early times at wavelengths consistent with the formation of FN$_n^{-\bullet}$ as determined by spectroelectrochemistry and femtosecond transient absorption spectroscopy of the model compounds without the NI acceptor. Once again, the 3D data sets were analyzed using global fitting to obtain the DADS (Figures S2 and S3 in the Supporting Information). The kinetic data associated with these spectra are given in Table 1. For DMJ-An−FN$_1$−NI, the first charge-separation step (CS1) from An$^{-\bullet}$ to FN$_1$ was too rapid to be resolved with our IRF.

Monitoring the appearance and decay of the NI$^{-\bullet}$ absorption bands yielded the time constants for the second charge-separation step (CS2) from FN$_1^{-\bullet}$ to NI (the defined effective charge-separation time) and charge recombination back to the ground state as τ_{CS2} = 0.9 ps and τ_{CR} = 54 ns, respectively. The charge-recombination time constants for all of the full D−B−A

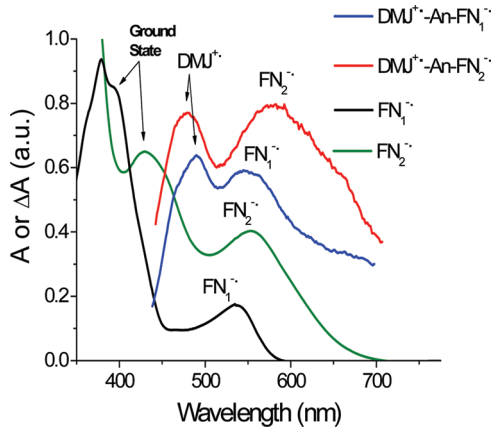

Figure 4. Spectroelectrochemical data of partially reduced FN$_1$ (black) and FN$_2$ (green) in DMF/0.1 M TBAPF$_6$ compared with the decay-associated difference spectra (DADS) obtained by singular value decomposition of the 3D transient absorption data sets (ΔA vs time and wavelength) for DMJ-An−FN$_1$ (blue) and DMJ-An−FN$_2$ (red) in toluene.

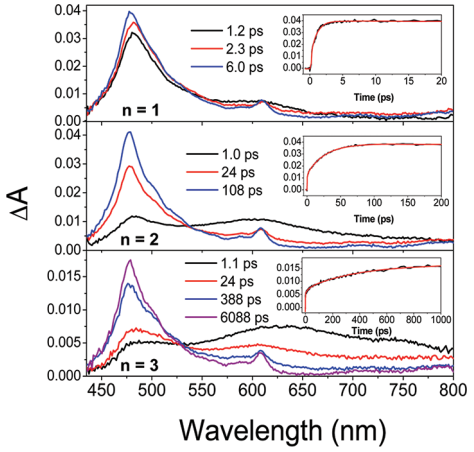

Figure 5. Transient absorption spectra of DMJ-An−FN$_n$−NI (n = 1−3) in toluene at 293 K at the indicated times following a 150 fs, 416 nm laser pulse. Insets: transient kinetics at 480 nm (black) and fits to the data (red).

dx.doi.org/10.1021/ja205913q | J. Am. Chem. Soc. 2012, 134, 4581−4588

Table 1. Electron-Transfer Time Constants

compound	τ_{CS1} (ps)	τ_{CS2} (ps)	τ_{CR} (ns)
DMJ-An−FN_1−NI	–	0.9 ± 0.3	54 ± 1
DMJ-An−FN_2−NI	5.6 ± 1.4	24 ± 3	420 ± 20
DMJ-An−FN_3−NI	13 ± 1	334 ± 40	5000 ± 400
DMJ-An−FN_1	21 ± 3	–	6.0 ± 0.2
DMJ-An−FN_2	30 ± 3	–	3.9 ± 0.2

systems were determined using nanosecond transient absorption spectroscopy, as they are significantly longer than 3 ns.[18] For DMJ-An−FN_n−NI (n = 2, 3), CS1 could be resolved, giving τ_{CS1} = 5.6 ps for n = 2 and 13 ps for n = 3. It should be noted here that τ_{CS1} for DMJ-An−FN_2−NI is faster than that for DMJ-An−FN_2. Since the transient absorption maximum of $FN_2^{-\bullet}$ is red-shifted relative to that of $FN_1^{-\bullet}$, there is some conjugation between the two FN bridge units within $FN_2^{-\bullet}$. Thus, attaching the NI acceptor to the second FN bridge unit can plausibly affect the electronic coupling between the FN units and the donor, thereby increasing the initial charge-separation rate in DMJ-An−FN_2−NI. Kinetic analysis of the $NI^{-\bullet}$ absorption bands showed that τ_{CS2} = 24 ps and τ_{CR} = 420 ns for DMJ-An−FN_2−NI and τ_{CS2} = 334 ps and τ_{CR} = 5 μs for DMJ-An−FN_3−NI. Additionally, transient absorption measurements on DMJ-An−FN_n (n = 1, 2) and DMJ-An−FN_n−NI (n = 1, 2) were performed in THF under the same conditions as discussed above. The transient absorption spectra and kinetic analyses are shown in Figure S4 in the Supporting Information.

Femtosecond IR Transient Absorption Spectroscopy. Visible pump/mid-IR probe spectroscopy was performed on DMJ-An−FN_n (n = 1, 2) and DMJ-An−FN_2−NI as an additional check on whether bridge reduction occurs in these molecules. The data were obtained in THF because toluene is too absorptive in the 1500−1800 cm^{-1} region. The data for DMJ-An−FN_n (n = 1 shown in Figure 6 and n = 2 shown in

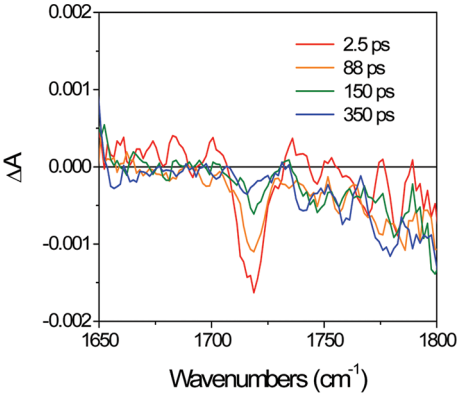

Figure 6. Femtosecond IR transient absorption spectra for DMJ-An−FN_1 in THF as a function of time following a 40 fs, 400 nm laser pulse.

Figure S5 in the Supporting Information) indicate that the 1720 cm^{-1} carbonyl stretching band[24] of FN_n is bleached with a time constant τ = 1.3 ps, which is longer than the 300 fs IRF of the apparatus. Therefore, the bleaching results from $FN_n^{-\bullet}$ formation rather than ^{1}*FN or ^{1}*FN_2 formation. Charge recombination in $DMJ^{+\bullet}$-An−$FN_n^{-\bullet}$ occurs with τ_{CR} =120 ps (n = 1) and 170 ps (n = 2). The transient IR data for DMJ-An−FN_2−NI are shown in Figure 7 and the kinetics is presented in Figure S5. The 1720 cm^{-1} bleaching appears with τ_{CS1} =1.1 ± 0.5 ps and decays with τ_{CS2} =19 ± 4 ps, which agrees to within

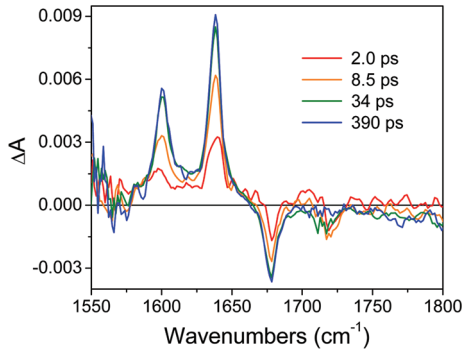

Figure 7. Femtosecond IR transient absorption spectra for DMJ-An−FN_2−NI in THF as a function of time following a 40 fs, 400 nm laser pulse.

experimental error with the appearance of the absorption changes at 1600, 1640, and 1677 cm^{-1} (τ_{CS2} =16.2 ± 0.5 ps) resulting from $NI^{-\bullet}$ formation. The charge-separation rate constants in more polar THF are somewhat larger than those observed in less polar toluene and are in excellent agreement with the corresponding visible transient absorption spectra and kinetics in THF (Figure S4 in the Supporting Information).

DISCUSSION

Determining the β Value. Femtosecond transient absorption measurements on DMJ-An−FN_n−NI (n = 1−3) at early times showed broad spectra consistent with the formation of $FN_n^{-\bullet}$ followed by formation of the characteristic $NI^{-\bullet}$ peaks. The DADS data (Figure S3 in the Supporting Information) revealed the sequence $DMJ^{+\bullet}$-$An^{-\bullet}$−FN_n−NI → $DMJ^{+\bullet}$-An−$FN_n^{-\bullet}$−NI → $DMJ^{+\bullet}$-An−FN_n−$NI^{-\bullet}$ for n = 2 and 3 but could not clearly separate a distinct $FN^{-\bullet}$ spectrum for n = 1, although the early-time spectra for n = 1 (Figure 5) suggested that $FN^{-\bullet}$ may have been present in very low concentrations. Complementary femtosecond transient IR data confirmed that the $FN_n^{-\bullet}$ bridge was reduced prior to NI reduction. A logarithmic plot of τ_{CS2} versus the donor−acceptor distance (r_{D-A}) is shown in Figure 8. The rate constant for electron arrival on NI decays exponentially with r_{D-A} with β = 0.34 $Å^{-1}$. This phenomenological β value *cannot be attributed to the usual superexchange mechanism* because the transient spectra show that stepwise electron transfer occurs in DMJ-An−FN_n−NI (n = 2, 3, and most likely also n = 1). In Figure 8 these data are compared with those obtained previously for the analogous

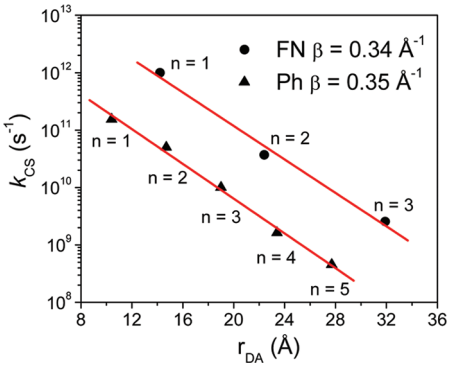

Figure 8. Plots of ln k_{CS2} vs r_{DA} for DMJ-An−FN_n−NI (n = 1−3) and DMJ-An−Ph_n−NI (n = 1−5). The red lines are the linear fits to the data.

dx.doi.org/10.1021/ja205913q | J. Am. Chem. Soc. 2012, 134, 4581−4588

molecules having *p*-phenylene (Ph_n) bridges.[25] The $DMJ^{+\bullet}$-$An-Ph_n^{-\bullet}-NI$ states are all virtual, so electron transfer to NI occurs strictly by the coherent superexchange mechanism. Interestingly, the β value for the FN_n bridge series is coincidentally nearly identical to that for the Ph_n bridge series, even though experiment shows that the charge-separation mechanisms differ.

Since there is clear spectroscopic evidence of bridge reduction prior to electron arrival at the terminal acceptor in the DMJ-An$-FN_n-$NI systems, it is logical to deduce that the electron is initially transferred from $An^{-\bullet}$ to the nearest FN unit. While the demonstrated red shifts in the $FN_2^{-\bullet}$ and $FN_3^{-\bullet}$ transient spectra relative to that of $FN^{-\bullet}$ indicate that the electron may be delocalized to a small degree beyond the first bridge unit, the delocalization is most likely modest because of the electrostatic attraction by $DMJ^{+\bullet}$. Since the individual bridge units are identical, we cannot experimentally differentiate between different FN sites. Nevertheless, by examining the data within the framework of several charge-hopping models, we can ascertain which of these models best describes the data.

As noted above, theory indicates that a significant phenomenological β value is possible for stepwise electron transfer if one or more of the following conditions is true: (1) the rates of charge hopping between independent bridge sites are the same but the rates of recombination to the donor and separation to the acceptor are significantly different; (2) the distance-dependent electrostatic attraction of the charges provides asymmetries in the forward and backward electron-hopping rates; and (3) significant electronic coupling between the bridge sites exists, which may cause injection of the electron onto the bridge to result in polaron formation.[16] For the molecules presented here, the modest red shift of the transient absorption maximum of $FN_2^{-\bullet}$ relative to that of $FN_1^{-\bullet}$ is consistent with some electronic interaction between the two FN bridge units within $FN_2^{-\bullet}$; however, the observed spectral changes are far smaller than those expected for a fully delocalized radical anion.[26] In addition, $|\Delta G| \leq 0.06$ eV for electron transfer between FN bridge sites (Figure 3 and Table S2 in the Supporting Information), and the total reorganization energy $\lambda = \lambda_S + \lambda_I$ is ~0.2 eV because the solvent reorganization energy (λ_S) for nonpolar toluene is approximately zero and the internal reorganization energy for electron transfer between FN bridge sites (λ_I) is ~0.2 eV (Table S3 in the Supporting Information). The resultant height of the activation barrier for electron transfer between FN bridge sites precludes substantial delocalization at room temperature. Thus, it is unlikely that polaron formation plays a significant role in the charge-transfer dynamics within DMJ-An$-FN_n-$NI, so we will focus on unbiased and biased charge hopping between discrete FN sites to model the data.

Unbiased Charge Hopping. If bidirectional electron hopping between each pair of FN units occurs at the same rate (k_h) and there is a substantial difference between the rates of charge removal from the bridge by recombination from the FN unit closest to the oxidized donor ($k_{1,D}$) and charge transfer to the acceptor from the FN unit adjacent to it ($k_{N,A}$) (Figure 9, $k_1 = k_2 = k_h$), kinetic modeling[14b] predicts that

$$k_{ET} = \frac{k_h e^{-\Delta E_{DB}/k_B T}}{\frac{k_h}{k_{N,A}} + \frac{k_h}{k_{1,D}} + N - 1} \quad (6)$$

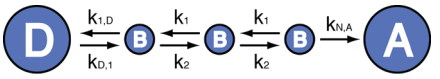

Figure 9. Kinetic schemes for the unbiased ($k_1 = k_2 = k_h$) and biased ($k_1 \gg k_2$) charge-hopping mechanisms following electron injection onto the bridge. k_h is the rate constant for electron hopping between adjacent bridge (B) units, while k_1 and k_2 are the electron-hopping rates toward the donor (D) and the acceptor (A), respectively. $k_{1,D}$ is the rate constant for charge transfer to the donor from the bridge unit adjacent to it, $k_{D,1}$ is the rate constant for charge transfer from the donor to the first bridge unit, and $k_{N,A}$ is the rate constant for charge transfer to the acceptor from the bridge unit adjacent to it.

where ΔE_{DB} is the energy change for charge injection from the donor to the first bridge site, k_B is Boltzmann's constant, T is the absolute temperature, and N is the number of bridge sites. The derivation of eq 6 using the conservation of flux can be found in the Supporting Information, eq 6 can be simplified to

$$k_{ET} = \frac{k_d e^{-\Delta E_{DB}/k_B T}}{1 + \frac{k_d}{k_h}(N-1)} \quad (7)$$

where $k_d = k_{1,D}k_{N,A}/(k_{1,D} + k_{N,A})$. The numerator of eq 7 does not depend on distance, but the denominator does; therefore, when $k_d(N-1)/k_h \ll 1$, the standard series expansion of the exponential function gives

$$\frac{1}{1 + \frac{k_d}{k_h}(N-1)} \approx e^{-k_d(N-1)/k_h} \quad (8)$$

Since $N = 1 + R/r$, where r is the distance between FN units and R is the overall distance over which the electron is transferred, eq 7 can be written as

$$k_{ET} = k_d e^{-\Delta E_{DB}/k_B T} e^{-k_d R/k_h r} \quad (9)$$

which gives $\beta = k_d/k_h r$ and $k_h = k_d/\beta r$. The data for DMJ-An$-FN_1$ and DMJ-An$-FN_1-$NI give $1/\tau_{CR} = k_{1,D} = 1.7 \times 10^8$ s^{-1} and $1/\tau_{CS2} = k_{N,A} = 1.1 \times 10^{12}$ s^{-1}, respectively, which in turn yield $k_d = 1.7 \times 10^8$ s^{-1}. Since the FN–FN distance is $r = 8$ Å and the measured value of β is 0.34 Å^{-1}, this model predicts that $k_h = 6.3 \times 10^7$ s^{-1}. However, the observed rates of electron arrival on NI ($1/\tau_{CS2}$) in DMJ-An$-FN_2-$NI and DMJ-An$-FN_3-$NI far exceed this predicted charge-hopping rate. Since the electron removal rates at the two ends of the bridge are substantially different, the failure of this simple kinetic model to describe the data indicates that the assumption of equal forward and backward hopping rates between the bridge sites is not fulfilled.

Biased Charge Hopping. As a result of the electrostatic attraction of $DMJ^{+\bullet}$ during electron transfer from $An^{-\bullet}$ to individual FN_n bridge units and ultimately to NI, the system can be described in terms of an asymmetric random walk.[27] The kinetic scheme is illustrated in Figure 9 ($k_1 \neq k_2$) and involves a treatment similar to that of the unbiased hopping model given above except that the rates of site-to-site hopping toward (k_1) and away (k_2) from the donor are assumed to be different. In this case, k_{ET} is given by

$$k_{ET} = \frac{k_1 e^{(-\Delta E_{DB}/k_B T)}}{\alpha} \xi^{R/r} = \frac{k_1 e^{(-\Delta E_{DB}/k_B T)}}{\alpha} e^{(R/r \ln \xi)} \quad (10)$$

dx.doi.org/10.1021/ja205913q | J. Am. Chem. Soc. 2012, 134, 4581–4588

where $\alpha = k_1/k_{N,A} - 1/(\xi - 1)$ and $\xi = k_2/k_1$ and it is assumed that $k_1 \gg k_2$ because in the case of electrostatic attraction, the rate of electron hopping toward the positively charged donor (k_1) is usually larger than that for hopping toward the neutral acceptor (k_2) (see the Supporting Information for the derivation). Comparison of eq 10 with the standard exponential distance dependence in eq 4 yields

$$\beta = -\frac{1}{r}\ln\left(\frac{k_2}{k_1}\right) \tag{11}$$

In this case, the rate constant for the electron-transfer process is also characterized by an exponential distance dependence. Using eq 11 with r = 8 Å and β = 0.34 Å^{-1}, one calculates $k_1/k_2 \approx 15$. The free energy changes for moving the electron from the first FN$^{-\bullet}$ to the other two FN sites in the presence of DMJ$^{+\bullet}$ for the series DMJ$^{+\bullet}$-An−FN$^{-\bullet}$−FN−FN → DMJ$^{+\bullet}$-An−FN−FN$^{-\bullet}$−FN → DMJ$^{+\bullet}$-An−FN−FN−FN$^{-\bullet}$ are ΔG = 0.06 and 0.03 eV, respectively (Table S2 in the Supporting Information). Thus, at room temperature, the expected values of $k_1/k_2 \approx e^{-\Delta G/k_BT}$ are 11 and 3.3, which are within an order of magnitude of the charge-hopping rate ratio predicted using the observed β value and the biased hopping model.

CONCLUSIONS

With the use of femtosecond transient absorption spectroscopy in the visible and mid-IR regions, the D−B−A systems studied here allowed us unequivocally to observe stepwise electron transfer while measuring an exponential distance dependence of the rate for the overall charge-separation reaction. The observed exponential distance dependence is attributed to electron injection onto the first FN unit followed by subsequent charge hopping within the FN$_n$ bridge biased by the electrostatic attraction of the charge on DMJ$^{+\bullet}$, with ultimate trapping at NI. This unusually high β value is likely a result of DMJ-An being a push−pull donor, where the charge-transfer excited state that is populated upon photoexcitation is dominated by a fully charge-separated radical ion pair state, DMJ$^{+\bullet}$-An$^{-\bullet}$.[17] The ultrafast formation of DMJ$^{+\bullet}$ provides an electrostatic attraction that slows electron injection from An$^{-\bullet}$ to the bridge and the subsequent electron hopping along the FN units to the NI trap site. These results show that D−B−A molecules designed to have stepwise, energetically downhill redox gradients do not necessarily exhibit wirelike behavior. Moreover, they highlight the need for a thorough knowledge of the mechanistic details of charge transport in D−B−A molecules that are utilized in systems for solar energy conversion and organic electronics, where wirelike properties are targeted.

ASSOCIATED CONTENT

Supporting Information

Details regarding the synthesis and characterization of DMJ-An−FN$_n$, redox potentials, absorption spectra, visible and IR transient absorption data, and derivations of eqs 6 and 10. This material is available free of charge via the Internet at http://pubs.acs.org.

AUTHOR INFORMATION

Corresponding Author

m-wasielewski@northwestern.edu; co@northwestern.edu

Notes

The authors declare no competing financial interest.

ACKNOWLEDGMENTS

This work was supported by the Chemical Sciences, Geosciences, and Biosciences Division, Office of Basic Energy Sciences, U.S. Department of Energy, under Grant DE-FG02-99ER14999. The authors thank Dr. Anton Trifonov for his help in assembling the femtosecond transient IR instrument.

REFERENCES

(1) Weiss, E. A.; Wasielewski, M. R.; Ratner, M. A. *Top. Curr. Chem.* **2005**, *257*, 103−133.
(2) (a) Jortner, J.; Bixon, M.; Langenbacher, T.; Michel-Beyerle, M. E. *Proc. Natl. Acad. Sci. U.S.A.* **1998**, *95*, 12759−12765. (b) Lewis, F. D.; Wu, T.; Zhang, Y.; Letsinger, R. L.; Greenfield, S. R.; Wasielewski, M. R. *Science* **1997**, *277*, 673−676.
(3) Gray, H. B.; Winkler, J. R. *Proc. Natl. Acad. Sci. U.S.A.* **2005**, *102*, 3534−3539.
(4) Kobori, Y.; Yamauchi, S.; Akiyama, K.; Tero-Kubota, S.; Imahori, H.; Fukuzumi, S.; Norris, J. R. Jr. *Proc. Natl. Acad. Sci. U.S.A.* **2005**, *102*, 10017−10022.
(5) (a) Hush, N. S.; Paddon-Row, M. N.; Cotsaris, E.; Oevering, H.; Verhoeven, J. W.; Heppener, M. *Chem. Phys. Lett.* **1985**, *117*, 8−11. (b) Paulson, B. P.; Miller, J. R.; Gan, W. X.; Closs, G. *J. Am. Chem. Soc.* **2005**, *127*, 4860−4868.
(6) (a) Weiss, E. A.; Ahrens, M. J.; Sinks, L. E.; Gusev, A. V.; Ratner, M. A.; Wasielewski, M. R. *J. Am. Chem. Soc.* **2004**, *126*, 5577−5584. (b) Goldsmith, R. H.; Sinks, L. E.; Kelley, R. F.; Betzen, L. J.; Liu, W.; Weiss, E. A.; Ratner, M. A.; Wasielewski, M. R. *Proc. Natl. Acad. Sci. U.S.A.* **2005**, *102*, 3540−3545. (c) Davis, W. B.; Svec, W. A.; Ratner, M. A.; Wasielewski, M. R. *Nature* **1998**, *396*, 60−63. (d) Albinsson, B.; Eng, M. P.; Pettersson, K.; Winters, M. U. *Phys. Chem. Chem. Phys.* **2007**, *9*, 5847−5864. (e) Winters, M. U.; Dahlstedt, E.; Blades, H. E.; Wilson, C. J.; Frampton, M. J.; Anderson, H. L.; Albinsson, B. *J. Am. Chem. Soc.* **2007**, *129*, 4291−4297.
(7) McConnell, H. M. *J. Chem. Phys.* **1961**, *35*, 508−515.
(8) (a) Marcus, R. A. *J. Chem. Phys.* **1965**, *43*, 679−701. (b) Jortner, J. *J. Chem. Phys.* **1976**, *64*, 4860−4867. (c) Hopfield, J. J. *Proc. Natl. Acad. Sci. U.S.A.* **1974**, *71*, 3640−3644.
(9) Bixon, M.; Jortner, J. *Adv. Chem. Phys.* **1999**, *106*, 3.
(10) Berlin, Y. A.; Hutchison, G. R.; Rempala, P.; Ratner, M. A.; Michl, J. *J. Phys. Chem. A* **2003**, *107*, 3970−3980.
(11) (a) Lembo, A.; Tagliatesta, P.; Guldi, D. M.; Wielopolski, M.; Nuccetelli, M. *J. Phys. Chem. A* **2009**, *113*, 1779−1793. (b) Wielopolski, M.; Atienza, C.; Clark, T.; Guldi, D. M.; Martin, N. *Chem.—Eur. J.* **2008**, *14*, 6379−6390. (c) Eng, M. P.; Martensson, J.; Albinsson, B. *Chem.—Eur. J.* **2008**, *14*, 2819−2826.
(12) (a) Paddon-Row, M. N.; Oliver, A. M.; Warman, J. M.; Smit, K. J.; de Haas, M. P.; Oevering, H.; Verhoeven, J. W. *J. Phys. Chem.* **1988**, *92*, 6958−6962. (b) Roest, M. R.; Oliver, A. M.; Paddon-Row, M. N.; Verhoeven, J. W. *J. Phys. Chem. A* **1997**, *101*, 4867−4871. (c) Lafolet, F.; Welter, S.; Popovic, Z.; De Cola, L. *J. Mater. Chem.* **2005**, *15*, 2820−2828.
(13) (a) Atienza-Castellanos, C.; Wielopolski, M.; Guldi, D. M.; van der Pol, C.; Bryce, M. R.; Filippone, S.; Martin, N. *Chem. Commun.* **2007**, 5164−5166. (b) Eng, M. P.; Albinsson, B. *Angew. Chem., Int. Ed.* **2006**, *45*, 5626−5629. (c) Giacalone, F.; Segura, J. L.; Martin, N.; Ramey, J.; Guldi, D. M. *Chem.—Eur. J.* **2005**, *11*, 4819−4834.
(14) (a) Grozema, F. C.; Tonzani, S.; Berlin, Y. A.; Schatz, G. C.; Siebbeles, L. D. A.; Ratner, M. A. *J. Am. Chem. Soc.* **2008**, *130*, 5157−5166. (b) Berlin, Y. A.; Grozema, F. C.; Siebbeles, L. D. A.; Ratner, M. A. *J. Phys. Chem. C* **2008**, *112*, 10988−11000. (c) Grozema, F. C.; Berlin, Y. A.; Siebbeles, L. D. A.; Ratner, M. A. *J. Phys. Chem. B* **2010**, *114*, 14564−14571.
(15) (a) Goldsmith, R. H.; DeLeon, O.; Wilson, T. M.; Finkelstein-Shapiro, D.; Ratner, M. A.; Wasielewski, M. R. *J. Phys. Chem. A* **2008**, *112*, 4410−4414. (b) Albinsson, B.; Martensson, J. *J. Photochem. Photobiol., C* **2008**, *9*, 138−155.
(16) (a) Henderson, P. T.; Jones, D.; Hampikian, G.; Kan, Y.; Schuster, G. B. *Proc. Natl. Acad. Sci. U.S.A.* **1999**, *96*, 8353−8358.

(b) Conwell, E. M. *Proc. Natl. Acad. Sci. U.S.A.* **2005**, *102*, 8795−8799. (c) Conwell, E. M.; Rakhmanova, S. V. *Proc. Natl. Acad. Sci. U.S.A.* **2000**, *97*, 4556−4560. (d) Kucherov, V. M.; Kinz-Thompson, C. D.; Conwell, E. M. *J. Phys. Chem. C* **2010**, *114*, 1663−1666.
(17) Lockard, J. V.; Ricks, A. B.; Co, D. T.; Wasielewski, M. R. *J. Phys. Chem. Lett.* **2010**, *1*, 215−218.
(18) Scott, A. M.; Ricks, A. B.; Colvin, M. T.; Wasielewski, M. R. *Angew. Chem., Int. Ed.* **2010**, *49*, 2904−2908.
(19) Giaimo, J. M.; Gusev, A. V.; Wasielewski, M. R. *J. Am. Chem. Soc.* **2002**, *124*, 8530−8531.
(20) Dance, Z. E. X.; Ahrens, M. J.; Vega, A. M.; Ricks, A. B.; McCamant, D. W.; Ratner, M. A.; Wasielewski, M. R. *J. Am. Chem. Soc.* **2008**, *130*, 830−832.
(21) Uckert, F.; Setayesh, S.; Müllen, K. *Macromolecules* **1999**, *32*, 4519−4524.
(22) Okada, T.; Fujita, T.; Kubota, M.; Masaki, S.; Mataga, N.; Ide, R.; Sakata, Y.; Misumi, S. *Chem. Phys. Lett.* **1972**, *14*, 563−568.
(23) Gosztola, D.; Niemczyk, M. P.; Svec, W.; Lukas, A. S.; Wasielewski, M. R. *J. Phys. Chem. A* **2000**, *104*, 6545−6551.
(24) Tanaka, S.; Kato, C.; Horie, K.; Hamaguchi, H. *Chem. Phys. Lett.* **2003**, *381*, 385−391.
(25) Scott, A. M.; Miura, T.; Ricks, A. B.; Dance, Z. E. X.; Giacobbe, E. M.; Colvin, M. T.; Wasielewski, M. R. *J. Am. Chem. Soc.* **2009**, *131*, 17655−17666.
(26) (a) Fujitsuka, M.; Tojo, S.; Shinmyozu, T.; Majima, T. *Chem. Commun.* **2009**, 1553−1555. (b) Lue, J.-M.; Rosokha, S. V.; Kochi, J. K. *J. Am. Chem. Soc.* **2003**, *125*, 12161−12171. (c) Nelsen, S. F.; Konradsson, A. E.; Weaver, M. N.; Telo, J. P. *J. Am. Chem. Soc.* **2003**, *125*, 12493−12501. (d) Penneau, J. F.; Stallman, B. J.; Kasai, P. H.; Miller, L. L. *Chem. Mater.* **1991**, *3*, 791−796. (e) Shida, T.; Iwata, S. *J. Chem. Phys.* **1972**, *56*, 2858−2864.
(27) Bar-Haim, A.; Klafter, J. *J. Chem. Phys.* **1998**, *109*, 5187−5193.